

Long-term timing evolution of four Anomalous X-Ray Pulsars

HAN-LONG PENG,¹ SHAN-SHAN WENG,¹ MING-YU GE,² SHI-QI ZHOU,³ ERBIL GÜGERCINOĞLU,⁴ WEN-TAO YE,² YOU-LI TUO,⁵ LIANG ZHANG,² JUAN ZHANG,² SHI-JIE ZHENG,² YU-JIA ZHENG,¹ AND XIAN-AO WANG⁶

¹*School of Physics and Technology, Nanjing Normal University, Nanjing, 210023, Jiangsu, China*

²*Key Laboratory of Particle Astrophysics, Institute of High Energy Physics, Chinese Academy of Sciences, Beijing 100049, China*

³*School of Physics and Astronomy, China West Normal University, Nanchong 637002, People's Republic of China*

⁴*School of Arts and Sciences, Qingdao Binhai University, Huangdao District, 266555, Qingdao, China*

⁵*Institut für Astronomie und Astrophysik, Universität Tübingen, Sand 1, D-72076 Tübingen, Germany*

⁶*Department of Astronomy, Yunnan University, Kunming 650500, China*

ABSTRACT

Anomalous X-ray pulsars (AXPs) and soft gamma-ray repeaters (SGRs) are believed to be manifestations of magnetars. Typically, AXPs exhibit higher X-ray luminosities, whereas SGRs are generally fainter and display significantly high signal-to-noise ratios only during their outburst phases. In this work, we report the long-term timing evolution of four AXPs: 1E 2259+586, 4U 0142+61, 1RXS J170849.0-400910 and 1E 1841-045, which were regularly monitored with *NICER* from 2017 to 2024. Over this period, we identify a total of 10 timing events. In addition to one glitch and one anti-glitch in 1E 2259+586 reported in literature, we detect another 8 new timing events: 5 glitches, 2 anti-glitches, and 1 unusual state transition event. Notably, both anti-glitches were observed in 4U 0142+61, making it the most frequent source of such events, and there is a hint of regular evolution in its pulse profile. In the case of 1RXS J170849.0-400910, it continues to exhibit pronounced high-frequency timing anomalies and undergoes a state transition event. Finally, we study the evolution of the pulse profiles and find that the profiles of 1E 2259+586 and 4U 0142+61 both evolve. This is consistent with the earlier finding that pulse profile evolution is a generic feature of magnetars.

Keywords: X-rays: stars — stars: magnetars

1. INTRODUCTION

The diagram of rotation period (P) versus spin-down rate (\dot{P}) is typically employed to classify pulsar populations. Magnetars occupy the upper-right region of the $P - \dot{P}$ diagram ($P \sim 2 - 12$ s and $\dot{P} \sim 10^{-13} - 10^{-10}$ s s $^{-1}$), representing the young neutron stars with the most intense magnetic fields (S. A. Olausen & V. M. Kaspi 2014). Historically, magnetars first appeared under the names of soft gamma-ray repeaters (SGRs) and anomalous X-ray pulsars (AXPs) (E. P. Mazets et al. 1979a; G. G. Fahlman & P. C. Gregory 1981). The detection of pulsations in SGRs and SGR-like bursts in AXPs (E. P. Mazets & S. V. Golenetskii 1979b; F. P. Gavriil et al. 2002) provided strong evidence for the unified magnetar model proposed by C. Thompson & R. C. Duncan (1995). This model attributes the energy sources of both phenomena to the ultra-strong magnetic

fields of neutron stars, rather than to spin-down power (C. Thompson & R. C. Duncan 1995, 1996). As of now, approximately 30 confirmed and candidate magnetars have been cataloged, with a comprehensive and regularly updated listing available in the McGill Magnetar Catalog⁷ (S. A. Olausen & V. M. Kaspi 2014).

One defining characteristic of magnetars is their rich and diverse radiative behavior, particularly at X-ray and soft gamma-ray energies. These are broadly divided into short-duration explosive events (bursts/flares, including giant flares) and outbursts. The former typically last from milliseconds to minutes, whereas the latter may decay over weeks to months or even years (V. M. Kaspi & A. M. Beloborodov 2017; P. Esposito et al. 2021; F. Coti Zelati et al. 2017). These episodes are often accompanied by timing anomalies (R. Dib et al. 2008), such as glitches. Sudden changes in spin frequency are known

as glitches, commonly seen in young, rotation-powered pulsars like the Crab pulsar (M. E. Lower et al. 2021; D. Antonopoulou et al. 2022). Unlike in ordinary rotation-powered pulsars, where glitches are usually discussed in terms of internal superfluid dynamics under an external electromagnetic torque, in magnetars the timing behavior is often intertwined with magnetic-field evolution and magnetically driven crustal activity. Within the magnetar framework, the strong and evolving magnetic field can build up stresses in the crust and induce fractures or plastic flow, which may make magnetars prone to glitches. Such crustal motions can perturb vortex-pinning conditions and the crust–superfluid coupling, triggering collective vortex unpinning and a rapid transfer of angular momentum to the crust. Consistent with this picture, glitches have been observed in a substantial fraction of magnetars in long-term timing campaigns (R. Dib & V. M. Kaspi 2014).

Most of the glitch events observed in pulsars are spin-up glitches characterized by a sudden increase in the rotational frequency. In addition to these, only a handful of pulsars have experienced more rare glitch events: slow glitches and delayed spin-ups (S. Q. Zhou et al. 2022a). Since the launch of *RXTE* and with the help of high resolution power imaging observations from space-borne satellites such as *Chandra*, *Swift*, and *XMM-Newton*, many of the unique timing and radiative behaviors of magnetars have been uncovered. In fact, magnetars have indeed been found to be a type of neutron star that frequently exhibit glitches. Perhaps more intriguingly, beyond ordinary glitches, an unique phenomenon was identified in magnetars: anti-glitches, also known as spin-down glitches, which occur in contrast to spin-up glitches and are characterized by a sudden decrease in rotational frequency. (R. F. Archibald et al. 2013). Although a few anti-glitch events have since been reported in a binary system (NGC 300 ULX-1) and two young, rotation-powered pulsars (P. S. Ray et al. 2019; S. Q. Zhou et al. 2024; Y. L. Tuo et al. 2024), nearly all known anti-glitches still occur in magnetars. The underlying reason why magnetars are particularly susceptible to glitches — and especially to anti-glitches — remains poorly understood. Furthermore, anti-glitches are far less common than normal glitches, and the relationship between the two types of events, as well as the rarity of anti-glitches, continues to be an open question. Two possible physical explanations for anti-glitches are the radial inward motion of superfluid vortex lines driven by crustquakes due to the evolution of the magnetic field within the crust (O. Akbal et al. 2015), or the time-variable coupling of magnetospheric and superfluid torques (E. Gügercioğlu & M. A. Alpar 2017).

Unlike rotation-powered pulsars, magnetars exhibit rich X-ray activity. Numerous studies have sought to investigate the connection between radiative activity and glitches, aiming to uncover a possible causal link. Establishing such a relationship would provide critical insights into the triggering mechanisms for magnetar activity and could help constrain theoretical models and geometric configurations of the timing behavior and the magnetic field structure within the crust and in the magnetosphere. For example, R. Dib & V. M. Kaspi (2014) performed a statistical analysis of five magnetars using 16 years of *RXTE* data. They found that while most radiative events, such as bursts, flux enhancements, and pulse profile changes, were accompanied by timing anomalies, only $\sim 30\%$ of timing anomalies were associated with observable radiative changes. The overlapping characteristics between spin-up and spin-down glitches, as well as between radiatively silent and active glitch events, and the similarity of AXP glitch behavior to that of the radio pulsar population, suggest a shared internal origin for all glitches, as has long been proposed for rotation-powered pulsars (P. W. Anderson & N. Itoh 1975; D. Pines & M. A. Alpar 1985). However, alternative views exist: some studies have proposed an external-torque interpretation, in which magnetospheric reconfigurations (e.g., changes in the twist/current system, partial opening/restructuring of field lines, or a variable particle wind) lead to abrupt changes in the spin-down torque and can generate timing signatures that may be interpreted as glitch-like events in phase-connected analyses (M. Lyutikov 2013; H. Tong 2014). Notably, R. F. Archibald et al. (2017) reported a net spin-down glitch in 4U 0142+61, which followed a decaying spin-up glitch. Their subsequent analysis indicated that nearly all spin-down glitches in magnetars were accompanied by radiative changes, further reinforcing the complexity of the glitch–activity relationship.

To date, numerous observational properties of magnetars have been discovered, and a number of review articles have summarized this progress. Some of them primarily focus on observational results (N. Rea & P. Esposito 2011; F. Coti Zelati et al. 2017), others on theoretical frameworks (R. Turolla et al. 2015; H. Tong 2023), and some offer a synthesis of both (P. Esposito et al. 2021; V. M. Kaspi & A. M. Beloborodov 2017). Despite these advances, many magnetar properties remain poorly understood. In particular, the triggering mechanisms of glitches and anti-glitches, as well as the underlying causal connection between glitches and radiative activity, remain elusive. The association of SGR J1935+2154 with FRB 200428 further suggests that at least some fast radio bursts (FRBs) – transient, ex-

tremely energetic, millisecond-duration bursts of radio waves – may originate from magnetars (B. Andersen et al. 2020; C. D. Bochenek et al. 2020), opening a new line of inquiry in magnetar astrophysics. Continued, systematic timing observations and the accumulation of glitch and activity samples are crucial for addressing these open questions. The Neutron Star Interior Composition Explorer (*NICER*) has provided sustained, high-cadence monitoring of a sample of magnetars over the past eight years. Its excellent time resolution and sensitivity in the soft X-ray band offer unique advantages for investigating the timing and pulse profile properties of magnetars. In this paper, we present a systematic timing analysis of four persistently bright magnetars (1E 2259+586, 4U 0142+61, 1RXS J170849.0-400910, and 1E 1841-045) based on *NICER* observations from 2017 to 2024. We focus on timing properties and pulse profile evolution. Analyses of flux variability and spectral properties will be addressed in a future study.

The structure of this paper is as follows: In Section 2, we provide a brief overview of the four AXPs. Section 3 describes the observations and the data reduction procedures. In Section 4, we summarize the analysis methods. Results are presented in Section 5, followed by a discussion of findings and conclusions in Section 6.

2. A SHORT REVIEW OF FOUR TARGETS

2.1. 1E 2259+586

1E 2259+586 was the first discovered AXP, with a spin period of approximately 6.8 s, located within the supernova remnant CTB 109 (G. G. Fahlman & P. C. Gregory 1981).

1E 2259+586 entered an outburst phase in 2002, during which a glitch occurred, accompanied by changes in pulsed profile, flux, and other properties (V. M. Kaspi et al. 2003; P. M. Woods et al. 2004). In 2007, the source experienced a second glitch, which, unlike the first, was in a radiatively quiet state and did not show any changes in the pulsed profile (R. Dib & V. M. Kaspi 2014). In 2009, a timing anomaly was also observed, accompanied by changes in pulsed flux and the pulsed profile (B. İçdem et al. 2012). In 2012, the source underwent its first anti-glitch, detected in *Swift* observations and accompanied by a short burst (R. F. Archibald et al. 2013). G. Younes et al. (2020) analyzed the observational data from *Swift* and *NICER* on this source from 2013 to 2019, identifying one glitch and one anti-glitch, both occurring in radiatively quiet states.

2.2. 4U 0142+61

4U 0142+61 is one of the brightest persistent magnetars, detected by the Uhuru mission (R. Giacconi et al.

1972), and later identified as a pulsar with a period of 8.7 s (G. L. Israel et al. 1994).

During a 16-year monitoring campaign with *RXTE*, the source entered an active phase in 2006, characterized by several short bursts and significant variations in timing behavior, pulse profile, and flux. R. Dib & V. M. Kaspi (2014) classified this event as a glitch candidate, while F. P. Gavriil et al. (2011a) suggested that it was a net spin-down glitch. In 2011, the source showed a large glitch, accompanied by a short burst detected by *Swift*. Additionally, *Swift* observed some short bursts from this source in 2015, during which an over-recovery glitch occurred, which resulted in a net spin-down because of significant recovery behavior following the initial spin-up glitch.

2.3. 1RXS J170849.0-400910

1RXS J170849.0-400910 (hereafter referred to as 1RXS J1708 for brevity) is an 11 s AXP first discovered as a pulsar by M. Sugizaki et al. (1997) by using ASCA data. Compared to 1E 2259+586 and 4U 0142+61, this source exhibits more frequent timing anomalies.

The first glitch was detected in 1999 (V. M. Kaspi et al. 2000), marking the first glitch ever observed in a magnetar – an expected phenomenon under the magnetar model. The second glitch was in 2001 with an exponential recovery (V. M. Kaspi & F. P. Gavriil 2003b), and the third glitch occurred in 2005 (R. Dib et al. 2008). All three events were radiatively quiet, showing no significant changes in pulse profile or flux. Israel et al. (2007) also reported several glitches, but R. Dib & V. M. Kaspi (2014) reclassified them as glitch candidates after considering timing noise. Additionally, P. Scholz et al. (2014) discovered a new glitch using *RXTE* and *Swift* data.

2.4. 1E 1841-045

1E 1841-045 is located at the center of the supernova remnant Kes 73, and was first classified as an AXP with a spin period of approximately 11.8 s (G. Vasisht & E. V. Gotthelf 1997). This source exhibits significant timing noise, with notable variations in its rotational frequency derivative on timescales of about a year. During the *RXTE* monitoring campaign, four glitches were observed in 2002, 2003, 2006, and 2007. Interestingly, all four glitches were radiatively quiet, showing no significant changes in radiative behavior—such as bursts or pulse profile variations (R. Dib et al. 2008; R. Dib & V. M. Kaspi 2014). It is worth noting that an anti-glitch was reported by S. Şaşmaz Muş et al. (2014), although this was not confirmed in the results of R. Dib & V. M. Kaspi (2014). In addition, H. An et al. (2015) presented

timing results from a three-year *Swift* observation campaign beginning in 2011, which revealed noisy timing behavior and large timing residuals. In August 2024, the source entered an active phase, which is markedly different from the previously quiet state. Almost all radiative behaviors changed, accompanied by a glitch (G. Younes et al. 2025).

3. OBSERVATION AND DATA REDUCTION

The Neutron Star Interior Composition Explorer (*NICER*) is a payload onboard the International Space Station, dedicated to studying neutron stars through soft X-ray (0.2–12 keV) timing observations (K. C. Gendreau et al. 2016). The Magnetars have been regularly monitored since the mission’s launch on 2017 June 3, with increased cadence after 2019. In this paper, we analyze all data from *NICER* observations of four Magnetars up to 2024. We use HEASOFT v6.33.2 to process the *NICER* data, initially employing the default standard procedure of `nicer12` (part of *NICERDAS* version v12) to generate cleaned and calibrated event files. We then apply `nicer13-lc` to extract light curves in the 12–15 keV band, and use `maketime` to filter out time intervals with count rates exceeding 0.2 counts s⁻¹, which are typically associated with particle-induced flaring. The resulting good time interval (GTI) file is then used to re-run `nicer12` to produce the final event file. Barycentric corrections are subsequently applied using the `barycorr` task. To generate the background spectra, which are later used in the pulse profile analysis, we use `nicer13-spect`, selecting the background model **3C50**. For a more detailed description of the *NICER* data processing pipeline, please refer to the webpage⁸.

After completing the data reduction, we select only those observations with exposure times longer than 50 seconds for timing analysis. Table 1 summarizes the basic properties of the sources, including the total number of *NICER* observations analyzed for each target, the start and end dates of the observations, and the energy bands used in the analysis.

Due to the limited number of *NICER* observations preceding the anti-glitch event in 1E 2259+586, we also include 20 archival *Swift* observations obtained before the event to better constrain the spin parameters (see Table 1). The cleaned event files are rebuilt using the task `xrtpipeline`, and only the Windowed Timing mode data with high temporal resolution (1.8 ms) are involved in this analysis. The source photons in the 0.5–10 keV band are extracted from a circular region with a radius of 20 pixels centered at the source posi-

tion, and then barycentric correction is performed using the task `barycorr`.

Similarly, to increase our data statistics and improve the accuracy of timing – particularly in determining the state transition events of 1RXS J170849.0-400910— we add two *IXPE* observations to our timing analysis for both 1E 2259+586 and 1RXS J170849.0-400910. We perform the data cleaning, region selection, and analysis using the software suite `ixpeobssim`, which is equipped with various tools to process level 2 event files and produce scientific results (L. Baldini et al. 2022). A circular region with a radius of 60" was selected for the extraction of source events, while an annular region with inner and outer radii of 180" and 240" was selected for background events. To improve the signal-to-noise ratio, we combined the data from all three detector units for the timing analysis. For a more detailed data processing pipeline regarding *IXPE*, readers can refer to these articles (H. L. Peng et al. 2024; R. Stewart et al. 2025; M. Rigoselli et al. 2025). As before, we use task `barycorr` to perform barycentric correction.

4. ANALYSIS

4.1. Timing Analysis

4.1.1. χ^2 searching and TOA calculation

We begin the timing analysis with a χ^2 search, identifying the spin frequency that yields the largest deviation from a uniform distribution in the folded pulse profile—quantified by the maximum χ^2 value—as the best-fit spin frequency for a barycenter-corrected, binned time series (M. Y. Ge et al. 2012). This search is performed approximately every 20 observations, with the exact interval adjusted based on the observation cadence and noise level. A preliminary ephemeris is constructed for each subset, and the corresponding pulse profiles are aligned and summed to generate a template pulse profile.

After obtaining the template pulse profile, we compute the phase shift ϕ_0 between each individual pulse profile and the template by means of cross-correlation (S. Q. Zhou et al. 2022b). The corresponding time of arrival (TOA) is then calculated using the following equation:

$$\text{TOA} = T_0 + \frac{\phi_0}{\nu}. \quad (1)$$

where T_0 denotes the time of the reference epoch for each observation (typically the starting point or midpoint) and ν is the spin frequency at that epoch. To estimate the uncertainty associated with each TOA, we introduce Poisson noise to each pulse profile to simulate 3000 noisy profiles, which are subsequently cross-correlated with the template. The uncertainty of the phase isulti-

⁸ https://heasarc.gsfc.nasa.gov/docs/nicer/analysis_threads/

Table 1. Summary of Spin Properties and X-ray Data

Parameter	1E 2259+586	4U 0142+61	1RXS J170849.0-400910	1E 1841-045
Frequency, ν (Hz)	0.1433	0.1151	0.0908	0.0847
$\dot{\nu}$ (10^{-13} Hz s $^{-1}$)	-0.097	-0.26	-1.68	-2.92
Magnetic field, B (10^{14} G)	0.59	1.3	4.7	7.0
Number of Analyzed <i>NICER</i> Observations	132	128	103	119
Total Exposure Time of <i>NICER</i> Observations (ks)	115.567	136.036	61.589	242.038
Date of the First Analyzed Observations	2018 Jan 17	2019 Mar 16	2019 Mar 14	2019 Mar 19
Date of the Last Analyzed Observations	2024 Oct 30	2024 Nov 13	2024 May 17	2024 Jun 26
Band Used for the Timing Analysis (keV)	0.8-8	0.7-10	0.7-10	0.7-10
Number of Analyzed <i>Swift</i> Observations	20	-	-	-
Total Exposure Time of <i>Swift</i> Observations (ks)	69.403	-	-	-
Date of the First Analyzed Observations	2017 Dec 7	-	-	-
Date of the Last Analyzed Observations	2019 Jan 7	-	-	-
Band Used for the Timing Analysis (keV)	0.5-10	-	-	-
The Observation ID of <i>IXPE</i>	02007899	-	01003199	-
The Exposure Time of <i>IXPE</i> Observations (ks)	328.530	-	837.633	-

NOTE—(a) The basic characteristics of the four sources are obtained from the McGill Magnetar Catalog webpage. (b) In this work, only two observations of *IXPE* are utilized; therefore, we simply list the observation ID and exposure time.

mately determined by the standard deviation of a series of returned values from the cross-correlation (R. Dib & V. M. Kaspi 2014).

4.1.2. Phase-coherent timing analysis

After obtaining the TOAs, we utilize the TEMPO2 software for timing analysis, which returns the spin parameters and residuals (G. B. Hobbs et al. 2006). We perform timing analysis in two different ways for four AXPs: partially phase-coherent timing (PPCT) and fully phase-coherent timing (FPCT). The former divides the data set into relatively short subsets and performs timing analysis by individually phase-connecting these subsets. This approach can reduce the effects of timing noise and covariances caused by polynomial fitting when determining the spin parameters, particularly when the data set is long enough to necessitate the use of many higher-order frequency derivatives. In contrast, FPCT phase-connects the entire data set, which enables us to confirm the results obtained from PPCT and obtain a more precise timing solution, especially regarding the parameter values of glitches (M. A. Livingstone et al. 2005).

Young pulsars—especially magnetars—often exhibit substantial timing noise, which can affect the measurement of intrinsic frequency parameters as well as the identification of glitches. To mitigate the impact of such noise on long-term timing evolution, PPCT is applied to segmented time intervals. By analyzing multiple shorter

time spans, we can more clearly trace the evolution of spin parameters (R. D. Ferdman et al. 2015). When no glitches are present, the long-term evolution of the TOAs in the phase domain can be modeled using a Taylor expansion:

$$\phi(t) = \phi_0 + \nu(t - t_0) + \frac{1}{2}\dot{\nu}(t - t_0)^2 + \frac{1}{6}\ddot{\nu}(t - t_0)^3 + \dots, \quad (2)$$

where ν , $\dot{\nu}$ and $\ddot{\nu}$ are the frequency, frequency derivative and the second derivative of frequency of the reference time t_0 , respectively (T. Wong et al. 2001).

We typically fit the timing model over intervals of approximately 100 days, with a \sim 50-day overlap between segments. These durations are also adjusted based on the level of timing noise and the TOA density. For most segments, we include only the spin frequency ν and its derivative $\dot{\nu}$ in the fit, except in cases of particularly strong timing noise. The reference epoch is chosen at the midpoint of each time segment (R. Dib & V. M. Kaspi 2014). If a glitch occurs, it manifests as a discontinuity in the residuals. PPCT segments are therefore chosen to avoid spanning glitch epochs.

Following the initial PPCT results, we apply FPCT to derive more accurate and continuous timing solutions (M. Ge et al. 2022; G. Younes et al. 2020). When a glitch occurs, Equation 2 is no longer valid, and the residuals deviate significantly. In such cases, FPCT assumes that

the phase residual model conforms to Equation:

$$\Delta\phi(t) = \Delta\nu\delta t + \frac{1}{2}\Delta\dot{\nu}\delta t^2 + \Delta\nu_d\tau \left[1 - e^{-\frac{\delta t}{\tau}}\right] \quad (3)$$

$$\delta t = t - t_g > 0$$

where t_g is the time when the glitch occurs, $\Delta\nu$ and $\Delta\dot{\nu}$ are the changes in frequency and frequency derivative, respectively. Sometimes, an exponential decay term needs to be added; τ is the duration for which the suddenly changed frequency $\Delta\nu_d$ returns to 0 (Y. L. Tuo et al. 2024; T. Wong et al. 2001). For each identified glitch, we perform FPCT using time intervals sufficiently long to capture the behavior both before and after the event, allowing us to determine refined timing parameters that account for both permanent and transient changes.

4.2. Pulse profile Analysis

For each source, we divide the observations into separate time segments based on the epochs of detected glitches, except for 1E 1841-045, where we used the observation gaps as segmentation points. For each segment, the corresponding ephemeris is used to fold the pulse profiles of all included observations. During this process, we calculate phase offsets between ephemerides to ensure that the resulting folded pulse profiles are phase-aligned across segments. To extract the net pulse profiles, we first estimate the background photon counts for each observation using its background spectrum. The background level is averaged over the phase intervals of each pulse profile, assuming that it remains stable within the short (few-second) exposure durations. Subtracting the estimated background yields the net pulse profile for each observation. We then sum the net pulse profiles from different time segments to obtain the net average pulse profiles. To compare profiles before and after a glitch, all pulse profiles are normalized by dividing by their respective mean count rates.

5. RESULTS

5.1. 1E 2259+586

A summary timing behavior of 1E 2259+586 as observed by *NICER* is shown in Figure 1. The long-term timing parameters of the source are listed in Table 2 and the pulse profiles are shown in Figure 2.

Panels (a) and (b) of figure 1 show that 1E 2259+586 exhibits low timing noise compared to other AXPs, which is consistent with previous findings (R. Dib & V. M. Kaspi 2014). As indicated by the black vertical dashed lines in figure 1, three large glitches occurred in 1E 2259+586 during the time span of our analysis.

Table 2. Spin parameters of 1E 2259+586 with glitches

Parameters	Value
R.A.	23:01:08.295
Decl.	+58:52:44.45
MJD range	58029.4-60672.0
Epoch (MJD)	58300
ν (Hz)	0.1432825964(1)
$\dot{\nu}$ (fHz \cdot s $^{-1}$)	-9.77(2)
t_{g1} (MJD)	58575
$\Delta\phi_{g1}$	-0.012(7)
$\Delta\nu_{g1}(10^{-8}$ Hz)	-8.95(5)
$\Delta\dot{\nu}_{g1}(10^{-16}$ Hz s $^{-1}$)	3.2(1)
$\Delta\nu_{d1}(10^{-8}$ Hz)	1.2(2)
τ_{d1} (day)	89(17)
$\Delta\nu_{g1}/\nu_{g1}(10^{-7})$	-6.25(3)
$\Delta\dot{\nu}_{g1}/\dot{\nu}_{g1}$	-0.033(1)
t_{g2} (MJD)	59780
$\Delta\phi_{g2}$	0.066(4)
$\Delta\nu_{g2}(10^{-7}$ Hz)	1.938(2)
$\Delta\dot{\nu}_{g2}(10^{-17}$ Hz s $^{-1}$)	-8.9(9)
$\Delta\nu_{g2}/\nu_{g2}(10^{-6})$	1.352(2)
$\Delta\dot{\nu}_{g2}/\dot{\nu}_{g2}$	0.009(1)
Residuals (ms)	48.554

NOTE—The subscripts g1 and g2 represent the parameters of the first and second glitch, respectively. The subscript d denotes the exponential decay term. The uncertainties of all the solutions to the spin parameters obtained using tempo2 in this paper are at the default confidence level of 1σ

A glitch event occurred in 1E 2259+586 shortly after the launch of *NICER*. Since only two data points are available before this glitch, we mark the time of the event with a black vertical line and treat it as the starting point of our timing analysis. Further details about this glitch can be found in G. Younes et al. (2020). The second timing event is an anti-glitch, which is also reported by G. Younes et al. (2020). However, we find that this anti-glitch is accompanied by an exponential decay phenomenon, which was not identified before. If this feature is not included, the subsequent TOAs cannot be well fitted, as shown in Figure 3. This discrepancy arises because their dataset covers only about 100 days post-event, insufficient to reveal the recovery trend. Indeed, when we use the same time span as in their study,

we reproduce their results. In this work, we use a sufficiently longer dataset and derive a more accurate spin parameters, as shown in Table 2. The timescale of the exponential recovery associated with this anti-glitch is estimated to be 89 ± 17 days. This exponential timescale can be explained by the creep response of vortex lines against flux tubes in the interior of a neutron star heated by magnetar activity, provided that the toroidal field in the core is a fraction of the polar magnetic field and the magnetar cools down by the direct Urca process (E. Gügercioğlu 2017). Furthermore, the increase in temperature due to magnetar burst activity can perturb the equilibrium angular velocity lag between the crust and the superfluid, leading to inward vortex motion and in turn anti-glitch (E. Gügercioğlu & M. A. Alpar 2016). Such a deviation from the steady-state vortex line distribution would produce a stronger radially outward vortex current, which is expected to lead to a large spin-up glitch via excess angular momentum transfer from the superfluid to the crust (E. Gügercioğlu & M. A. Alpar 2019). Indeed, following the anti-glitch, we detect a new glitch.

Owing to the low timing noise, a straightforward ephemeris is able to fit all TOAs covering a 7-year span, as shown in Table 2. Panel (c) of figure 1 displays the residuals after subtracting our best-fit model.

We divide the data into three segments based on the epochs of the glitches (excluding the two early observations prior to the first glitch), and construct an average pulse profile for each segment. Each profile consists of 50 phase bins based on the corresponding ephemeris shown in Table 3. We normalize and compare the pulse profiles before and after each glitch, as shown in Figure 2. The pulse profile of 1E 2259+586 is characterized by two peaks of varying heights, consistent with previous studies. We find that although there are no significant characteristic changes (such as the transition from single-peaked to multi-peaked profiles observed before and after the 1E 1841-045 burst, as described below), the pulse profiles accumulated over a longer period do exhibit changes, as reflected in the statistical values from the chi-squared test (Table 9). This is consistent with the previous idea that magnetars exhibit slow, low-level changes, which can only be detected by summing the pulse profiles over an extended period of time (R. Dib et al. 2008; R. Dib & V. M. Kaspi 2014).

5.2. 4U 0142+61

A summary of the behavior of 4U 0142+61 as observed by *NICER* is shown in Figure 4. The long-term timing parameters of the source are presented in Table 4 and the pulse profiles are shown in Figure 5.

As can be seen in figure 4, two notable timing events occurred during the time span of our analysis, marked by the vertical dashed lines.

Over the seven-year *NICER* monitoring campaign, 4U 0142+61 exhibited two timing anomaly events occurring at closely spaced epochs (59540 and 59850 MJD), suggesting that glitch events in this source do not follow a regular periodic pattern. Interestingly, both timing anomalies are anti-glitches, with $\Delta\nu_{g1} = -1.25(9) \times 10^{-8}$ Hz and $\Delta\nu_{g2} = -5.42(9) \times 10^{-8}$ Hz. The magnitudes of the frequency change are consistent with earlier observations. R. F. Archibald et al. (2017) previously reported two similar spin-down glitches in this source. Including these two spin-down glitch events, source 4U 0142+61 has become the one with the highest cyan rate of such occurrences; however, the underlying cause of this phenomenon remains unknown. Probably the strong toroidal magnetic field within the crust is evolving in a way that can intermittently release magnetic stress, thereby facilitating vortex-mediated transfer of angular momentum from the magnetar's crust to its interior (C. Thompson et al. 2000). Such stress-release episodes may be radiatively loud, producing bursts/outbursts, but they may also be radiatively quiet and leave little or no detectable radiative signature. During the *NICER* observation period, the timing behavior of 4U 0142+61 is relatively stable, enabling the use of a single timing solution to fit all TOAs, as listed in Table 4.

We divide the data into three intervals based on the epochs of the glitches and construct an average pulse profile for each segment. Each profile consists of 50 phase bins based on the corresponding ephemeris shown in Table 5. We normalize and compare the pulse profiles before and after each glitch, as shown in Figure 5. The pulse profile of 4U 0142+61 is also characterized by two peaks of varying heights, consistent with previous results. Our analysis reveals that the pulse profile of source 4U 0142+61 demonstrates a regular evolutionary trend, marked by an upward shift in the valley between the secondary peak and the main peak (a finding consistently confirmed by segmenting the data into additional time intervals). Notably, the main peak exhibits significant changes before and after the second glitch event, whereas no such changes are observed around the first glitch. This suggests that the observed variation is not a result of regular evolution. The chi-squared test values (Table 9) also indicate that there are changes in the pulse profiles. This is consistent with the previous idea that magnetars exhibit slow, low-level changes, which can only be detected by summing the pulse profiles over

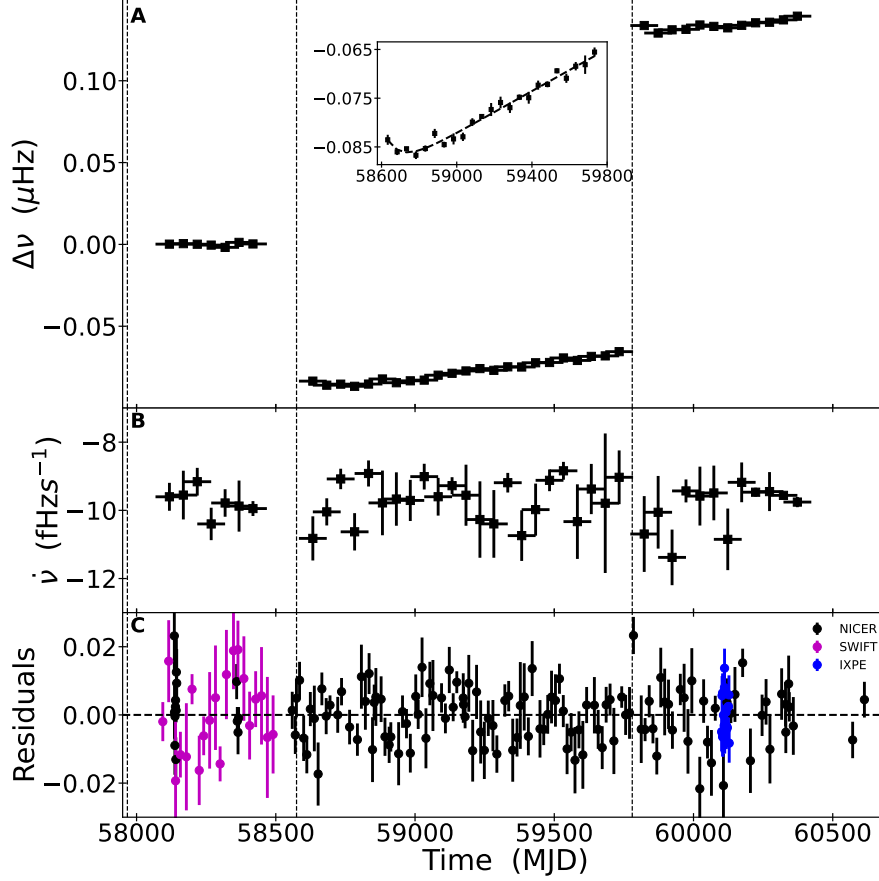


Figure 1. The long-term timing evolution of 1E 2259+586. Three vertical dashed lines represent the times of the glitches within the *NICER* observation range. Panel(A), Frequency as a function of time with a linear trend in frequency subtracted. The inset graph zooms in on the results of the anti-glitch, revealing the existence of an exponential term. Panel(B), Frequency derivative as a function of time. Panel(C), The timing residuals of all TOAs, black, magenta, and blue data represent from *NICER*, *Swift* and *IXPE*, respectively.

Table 3. Spin parameters of 1E 2259+586 without glitches

Parameters	R.A.	Decl.	
Value	23:01:08.295	+58:52:44.45	
Parameters	S1	S2	S3
MJD range	58068-58584	58584-59783	59783-60677
Epoch (MJD)	58300	59000	60000
ϕ_0	0.832(2)	0.2612(7)	0.205(1)
ν (Hz)	0.1432825964(1)	0.14328192855(6)	0.1432813039(1)
$\dot{\nu}$ (fHz \cdot s $^{-1}$)	-9.77(1)	-9.467(3)	-9.534(6)
Residuals (ms)	52.397	74.030	51.778

NOTE—S1, S2, and S3 represent the three time ranges obtained by using the glitch epochs as segmentation points.

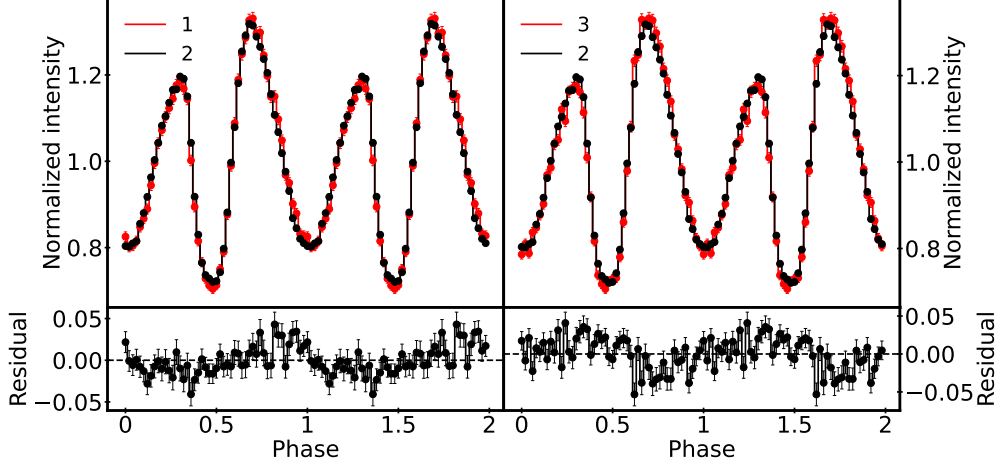


Figure 2. Comparison results of normalized pulse profiles of 1E 2259+586. The numbers 1-3 represent the average pulse profiles for the three time segments, divided based on the glitch events shown in Figure 1 (with the first glitch excluded). The residuals for each pair of normalized pulse profiles, obtained by subtracting one profile from the other, are plotted below the corresponding panels.

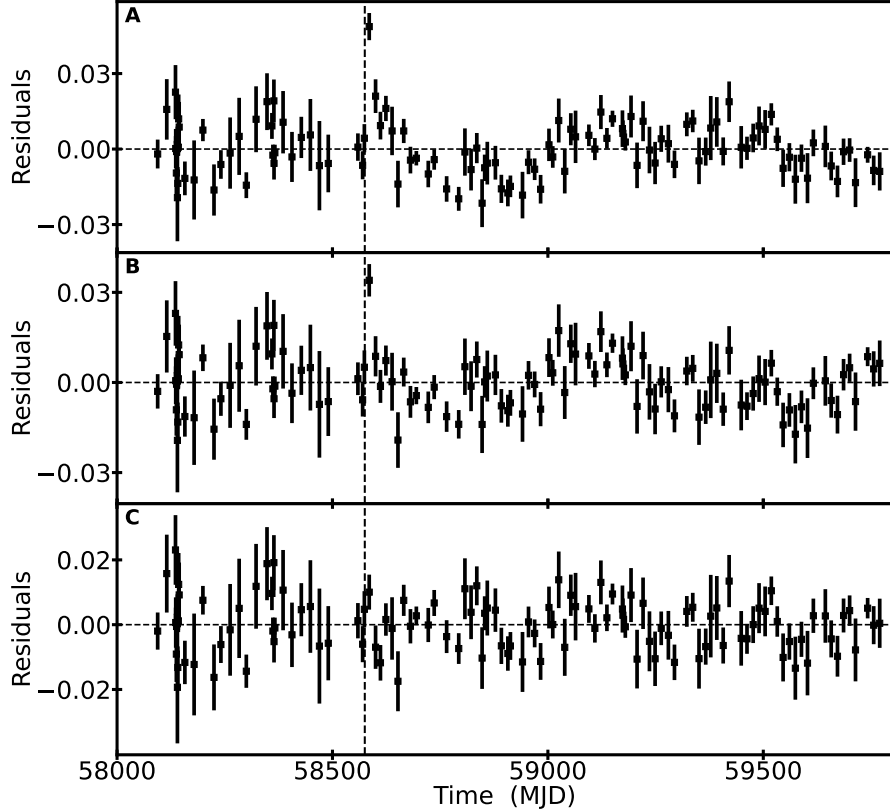


Figure 3. The timing residuals of the anti-glitch for 1E 2259+586 obtained from three different models. Panel(A), excluding the exponential term, the model utilized only ν , $\dot{\nu}$, $\Delta\nu$, $\Delta\dot{\nu}$, with an RMS residual of 68.988 ms. Panel(B), the second derivative of frequency $\ddot{\nu}$ was added to the analysis from Panel(A), with an RMS residual of 57.448 ms. Panel(C), the exponential term $\Delta\nu_d$ was added to the analysis from Panel(A), with an RMS residual of 46.865 ms.

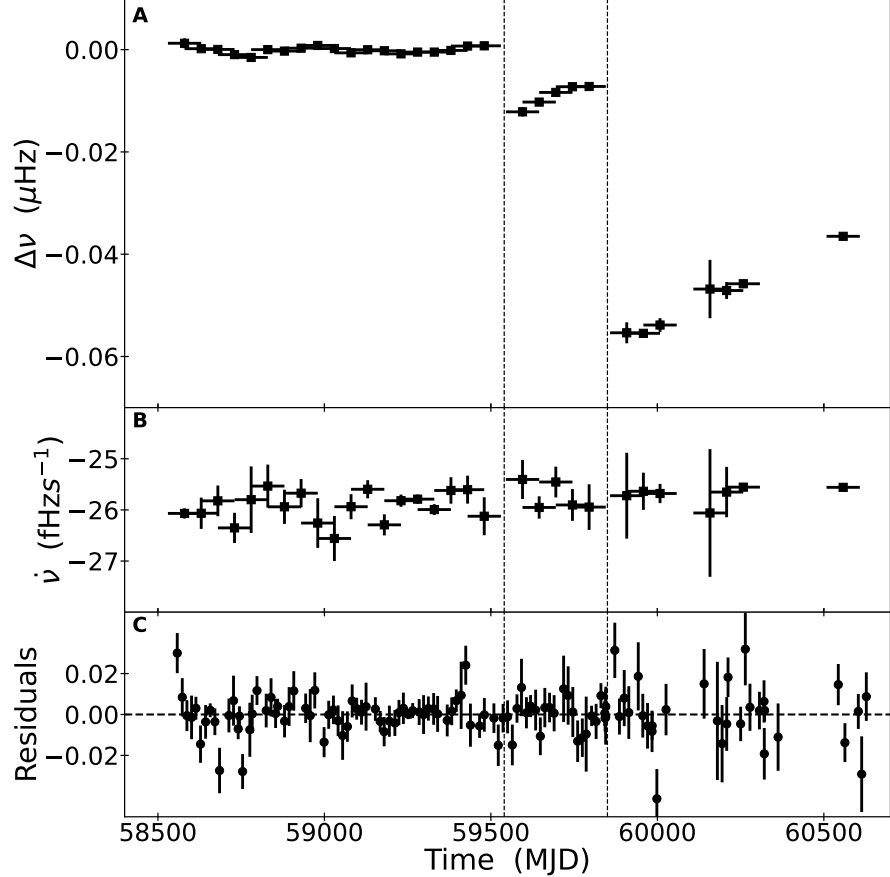


Figure 4. The long-term timing evolution of 4U 0142+61. Two black vertical dashed lines represent the times of the glitches within the *NICER* observation range. Panel(A), Frequency as a function of time with a linear trend in frequency subtracted. Panel(B), Frequency derivative as a function of time. Panel(C), The timing residuals of all TOAs.

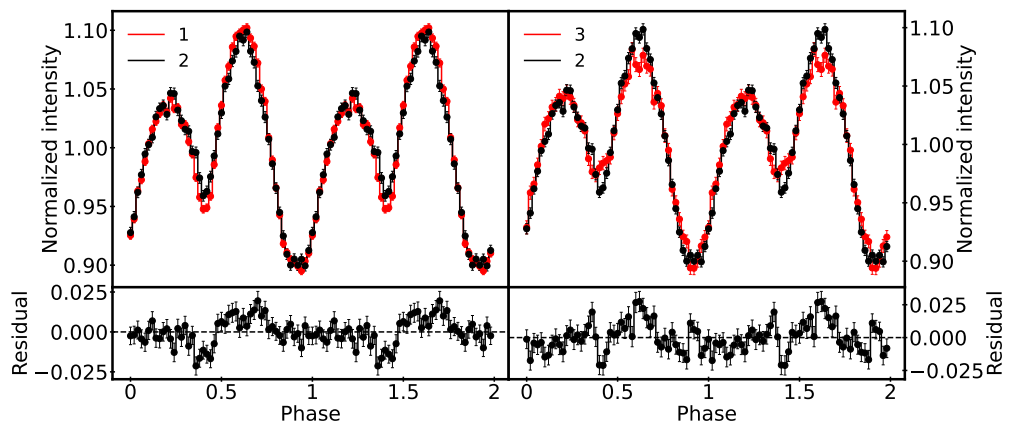


Figure 5. Comparison results of normalized pulse profiles of 4U 0142+61. The numbers 1-3 represent the average pulse profiles for the three time segments, divided based on the glitch events shown in Figure 4. The residuals for each pair of normalized pulse profiles, obtained by subtracting one profile from the other, are plotted below the corresponding panels.

Table 4. Spin parameters of 4U 0142+61 with glitches

Parameters	Value
R.A.	01:46:22.21
Decl.	+61:45:03.8
MJD range	58504.0-60730.1
Epoch (MJD)	59000
ν (Hz)	0.11508073213(4)
$\dot{\nu}$ (10^{-14} Hz s $^{-1}$)	-2.5914(3)
t_{g1} (MJD)	59540
$\Delta\phi_{g1}$	-0.002(6)
$\Delta\nu_{g1}$ (10^{-8} Hz)	-1.25(9)
$\Delta\dot{\nu}_{g1}$ (10^{-16} Hz s $^{-1}$)	2.8(6)
$\Delta\nu_{g1}/\nu_{g1}$ (10^{-7})	-1.09(9)
$\Delta\dot{\nu}_{g1}/\dot{\nu}_{g1}$	-0.011(2)
t_{g2} (MJD)	59850
$\Delta\phi_{g2}$	-0.044(6)
$\Delta\nu_{g2}$ (10^{-8} Hz)	-5.42(9)
$\Delta\dot{\nu}_{g2}$ (10^{-16} Hz s $^{-1}$)	1.0(7)
$\Delta\nu_{g2}/\nu_{g2}$ (10^{-7})	-4.71(8)
$\Delta\dot{\nu}_{g2}/\dot{\nu}_{g2}$	-0.004(3)
Residuals (ms)	61.515

NOTE—The subscripts g1 and g2 represent the parameters of the first and second glitch, respectively.

an extended period of time (R. Dib et al. 2008; R. Dib & V. M. Kaspi 2014).

5.3. 1RXS J170849.0-400910

A summary of the timing behavior of 1RXS J1708 as observed by *NICER* is shown in Figure 6. The long-term timing parameters are listed in Table 6, and the pulse profiles are presented in Figure 7.

Panels (a) and (b) of figure 6 show that 1RXS J1708 underwent multiple timing discontinuities. Four glitches are marked by vertical dashed lines, and a state transition region is highlighted between the vertical solid lines.

1RXS J1708 remains one of the most prolific sources in terms of timing anomalies. During the *NICER* observation period, the source exhibits four distinct glitch events. The first event displays the largest frequency change of 137 nHz, while subsequent events show smaller magnitudes. It is noteworthy that a special evolutionary behavior occurs around 59800 MJD, between the two vertical solid lines. At first glance, this behavior resembles two consecutive spin-down glitches. However, upon closer inspection, we identify it as a gradual decrease in

spin frequency accompanied by a gradual decline in the frequency derivative – reminiscent of the slow glitch phenomenon reported by S. Q. Zhou et al. (2022a). However, we do not refer to it as a slow anti-glitch, as overly detailed naming conventions may hinder the search for patterns. Instead, we describe this episode as a state transition (encompassing a slow glitch-like event), possibly caused by a change in the torque acting on the star. A plausible candidate for this state transition is that, assuming the magnetar undergoes frequent jumps caused by superfluid vortex discharges induced by crustquakes, the heating resulting from the dissipation of mechanical and magnetic field energy changes the direction of movement of the vortex lines. The observed sinusoidal-like oscillations in deceleration rate and spin frequency are consistent with the effect of time-varying internal torque applied to the crust, arising from changed configuration of vortex lines (E. Gügercioğlu et al. 2023).

We divide the dataset into seven segments based on the glitch epochs, including the interval marked by the solid lines, and construct an average pulse profile for each. Each profile consists of 32 phase bins based on the corresponding ephemeris shown in Table 7. After normalization, the pulse profiles before and after each event are compared, as shown in Figure 7. In the 0.5–8 keV energy range, the pulse profile of 1RXS J1708 consistently exhibits a stable single-peaked morphology. We do not find significant changes in the pulse profiles, except for the last set (which includes only six observations). The results of the chi-squared test are presented in Table 9.

5.4. 1E 1841-045

A summary of the behavior of 1E 1841-045 as observed by *NICER* is shown in Figure 8. The long-term timing parameters of the source are listed in Table 8 and the pulse profiles are presented in Figure 9.

Panels (a) and (b) of figure 8 reveal that 1E 1841-045 is a timing-noisy source: its rotational frequency derivative exhibits significant variations on timescales of years.

Due to observational constraints such as Sun-avoidance angles, *NICER*'s coverage of 1E 1841-045 is subject to periodic gaps, lasting approximately one-quarter to one-third of each year. Combined with the intrinsic timing noise of the source, this makes timing analysis more challenging than for the other three magnetars in our sample. We do not identify any definitive glitch events during the observation period. Although some apparent discontinuities are present before and after the data gaps, we are unable to determine their precise nature—whether they correspond to actual glitches,

Table 5. Spin parameters of 4U 0142+61 without glitches

Parameters	R.A.	Decl.	
Value	01:46:22.21	+61:45:03.8	
Parameters	S1	S2	S3
MJD range	58500-59546	59546-59860	59860-60700
Epoch (MJD)	59000	59700	60200
ϕ_0	0.054(1)	0.918(2)	0.843(3)
ν (Hz)	0.11508073213(3)	0.1150791561(1)	0.1150779975(1)
$\dot{\nu}$ (10^{-14} Hz s $^{-1}$)	-2.5914(3)	-2.564(5)	-2.554(1)
Residuals (ms)	54.496	50.639	104.110

NOTE—S1, S2, and S3 represent the three time ranges obtained by using the glitch epochs as segmentation points.

Table 6. Spin parameters of 1RXS J170849.0-400910 with glitches

Parameters	R.A.	Decl.			
Value	17:08:46.87	-40:08:52.44			
Parameters	S1	S2	S3	S4	mode-switching
MJD range	58550-59290	58760-59535	59290-59760	59870-60510	59760-59870
Epoch (MJD)	58650	59000	59400	60100	59800
ν (Hz)	0.0908133608(5)	0.0908084107(3)	0.0908026601(5)	0.0907921232(4)	0.090796633(2)
$\dot{\nu}$ ($\times 10^{-13}$ Hz s $^{-1}$)	-1.665(2)	-1.6881(2)	-1.694(2)	-1.6621(8)	-2.27(3)
$\ddot{\nu}$ ($\times 10^{-23}$ Hz s $^{-2}$)	2.0(5)	1.9(5)	-	-	1025(151)
Parameters	G1	G2	G3	G4	mode-switching
t_g (MJD)	58755	59290	59540	60200	-
$\Delta\phi_g$	0.077(9)	0.040(9)	-0.01(3)	0.08(2)	-
$\Delta\nu_g$ ($\times 10^{-8}$ Hz)	13.7(2)	8.4(2)	2.9(6)	2.2(3)	-
$\Delta\dot{\nu}_g$ ($\times 10^{-15}$ Hz s $^{-1}$)	2.9(3)	1.3(2)	1.4(5)	1.4(2)	-
$\Delta\nu_g/\nu_g$ ($\times 10^{-7}$)	15.1(2)	9.2(2)	3.2(7)	2.5(3)	-
$\Delta\dot{\nu}_g/\dot{\nu}_g$	0.018(2)	0.007(1)	-0.008(3)	0.008(1)	-
Residuals (ms)	96.630	98.523	118.789	80.238	53.456

NOTE—S1 to S4 represent the four time ranges that include G1 to G4.

gradual state transitions (as in the case of 1RXS J1708), or are simply artifacts of timing noise. Therefore, we divide the data based on these gaps and provide independent ephemerides and corresponding pulse profiles for each segment, as shown in Table 8 and Figure 9.

It is worth noting that although the fourth vertical dashed line in Figure 8 does not fall within a data gap, it is followed by only seven data points before the next gap, and the folded profile in this region has a low signal-to-noise ratio. Thus, we do not classify this feature as a glitch. Instead, we treat the adjacent segments as independent ephemerides for fitting purposes. Despite the lack of clear glitch identification, the observed long-term trends in spin frequency and its derivative suggest that

the rotational behavior of 1E 1841-045 has undergone irregular changes.

We segment the dataset into seven intervals based on the timing gaps (including the segment associated with the fourth vertical dashed line) and construct an average pulse profile for each. Each profile consists of 32 bins based on the ephemeris. We normalize and compare the pulse profiles before and after each line, as shown in Figure 9. The pulse profile of 1E 1841-045 is characterized by a relatively stable single-peaked structure, accompanied by a small bump on the trailing edge. We do not find significant changes in the pulse profiles and the results of the chi-squared test are presented in Table 9.

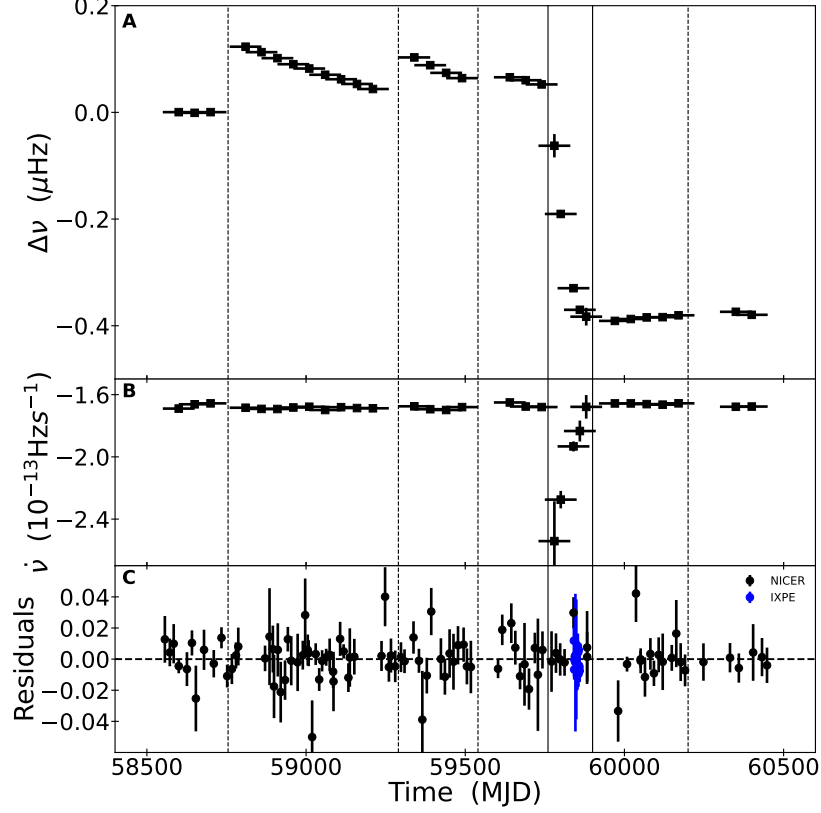


Figure 6. The long-term timing evolution of 1RXS J1708. Four vertical dashed lines represent the times of the glitches within the *NICER* observation range. Between the two vertical solid lines, a state transition scenario occurred. Panel(A), Frequency as a function of time with a linear trend in frequency subtracted. Panel(B), Frequency derivative as a function of time. Panel(C), The timing residuals of all TOAs, black and blue data represent from *NICER* and *IXPE*, respectively.

Table 7. Spin parameters of 1RXS J170849.0-400910 without glitches

Parameters	R.A.	Decl.					
Value	17:08:46.87	-40:08:52.44					
Parameters	S1	S2	S3	S4	S5	S6	S7
MJD range	58550-58755	58755-59290	59290-59535	59535-59760	59760-59870	59870-60200	60200-60510
Epoch (MJD)	58650	59000	59400	59700	59800	60100	60400
ϕ_0	0.063(3)	0.734(2)	0.957(3)	0.398(5)	0.676(5)	0.483(3)	0.222(5)
ν (Hz)	0.090813358(1)	0.0908084107(3)	0.0908026601(4)	0.090798317(2)	0.090796633(3)	0.0907921232(5)	0.0907878128(5)
$\dot{\nu}$ (10^{-13} Hz s $^{-1}$)	-1.666(3)	-1.6881(2)	-1.695(1)	-1.679(6)	-2.27(3)	-1.6621(9)	-1.676(1)
$\ddot{\nu}$ (10^{-22} Hz s $^{-2}$)	3(1)	-0.19(4)	-	-	102(15)	-	-
Residuals (ms)	82.463	78.647	107.247	131.581	53.455	88.244	34.840

NOTE—S1 to S7 represent the seven time ranges obtained by using the vertical lines in Figure 6 as segmentation points.

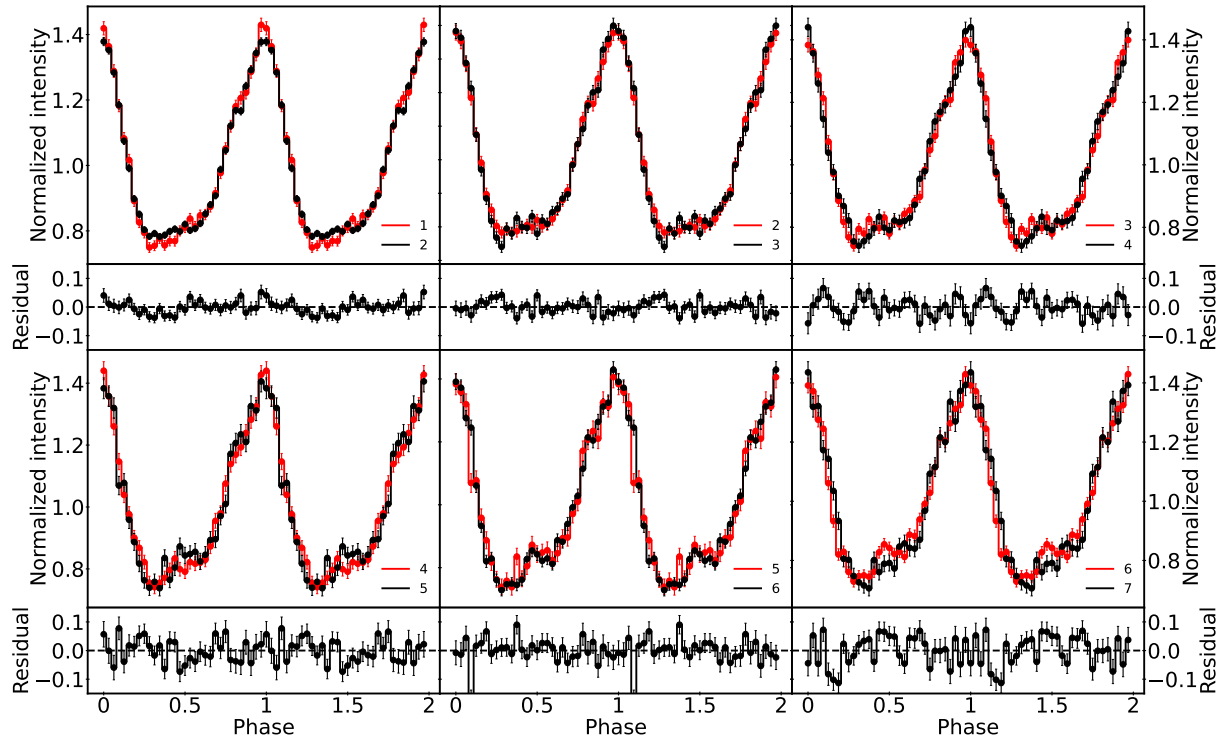


Figure 7. Comparison results of normalized pulse profiles of 1RXS J1708. The numbers 1-7 represent the average pulse profiles for the seven time segments, divided based on the vertical lines shown in Figure 6. The residuals for each pair of normalized pulse profiles, obtained by subtracting one profile from the other, are plotted below the corresponding panels.

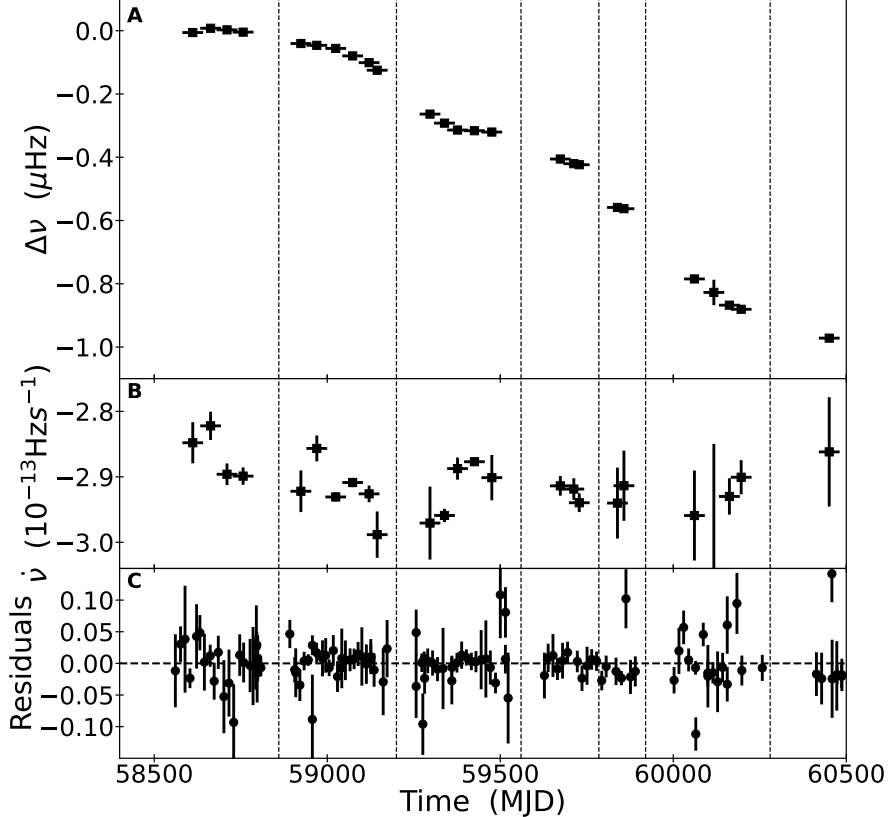


Figure 8. The long-term timing evolution of 1E 1841-045. Panel(A), Frequency as a function of time with a linear trend in frequency subtracted. Panel(B), Frequency derivative as a function of time. Panel(C), The timing residuals of all TOAs.

Importantly, following the time span analyzed here, 1E 1841-045 entered an active phase, during which an outburst occurred, accompanied by a short burst, a flux enhancement, and a glitch. Notably, its pulse profile underwent a dramatic transformation. Unlike the gradual evolutionary changes observed earlier, the profile shifted from a quasi-single-peaked to a complex multi-peaked morphology, as illustrated in Figure 10. For detailed timing and spectral analysis of this event, refer to the report by G. Younes et al. (2025). Additional analysis by Fu et al. (2026, in preparation) will be presented in a forthcoming publication.

6. DISCUSSION AND SUMMARY

We present, for the first time, a systematic timing and pulse profile analysis from *NICER*'s regular monitoring of four AXPs (1E 2259+586, 4U 0142+61, 1RXS J1708, and 1E 1841-045) over roughly 7 years. This has yielded a rich data set, significantly expanding the sample of glitch events in magnetars. During this time span, each source exhibited its own unique rotational behavior. For example, 1E 2259+586 is a very stable rotator, while 1RXS J1708, in contrast, is a frequent glitcher, and 4U 0142+61 stands out even more due to its anti-

glitch behavior. That said, even among magnetars, each source retains its distinct characteristics in terms of radiation and spin evolution. Systematic analysis not only reveals clear common behaviors but also highlights differences between sources, which can help explore the underlying triggering mechanisms. This is crucial for developing a coherent theory to explain magnetar phenomenology.

Specifically, we identify a total of 10 timing events. In addition to one glitch and one anti-glitch in 1E 2259+586 that have already been reported (G. Younes et al. 2020), we discover 8 new events: 1E 2259+586 exhibits another glitch, and in the previous anti-glitch event, we find an exponential decay term, which was not recognized in earlier reports. 4U 0142+61 shows two spin-down glitches. 1RXS J1708 undergoes four glitches and one unique state transition event. Due to observational gaps, we do not identify specific glitch events in 1E 1841-045. Detailed statistics of the timing events are presented in Table 10.⁹

⁹ After the range of data we analyzed, 1E 1841-045 enters an active phase accompanied by a glitch event, which G. Younes

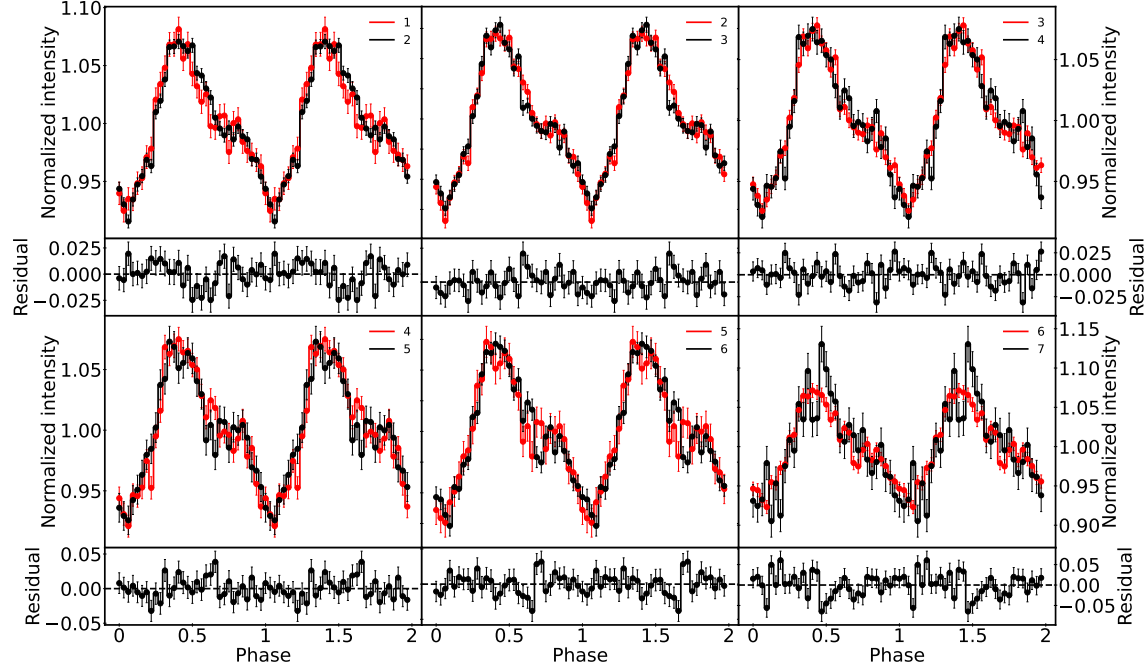


Figure 9. Comparison results of normalized pulse profiles of 1E 1841-045. The numbers 1-7 represent the average pulse profiles for the seven time segments, divided based on the vertical dashed lines shown in Figure 8. The residuals for each pair of normalized pulse profiles, obtained by subtracting one profile from the other, are plotted below the corresponding panels.

Table 8. Spin parameters of 1E 1841-045

Parameters	R.A.	Decl.							
Value	18:41:19.343	-04:56:11.16							
Parameters	S1	S2	S3	S4	S5	S6	S7		
MJD range	58530-58860	58860-59200	59230-59570	59600-59790	59790-59910	59980-60290	60410-60490		
Epoch (MJD)	58623	59000	59400	59700	59850	60050	60450		
ϕ_0	0.026(9)	0.727(5)	0.058(7)	0.625(7)	0.066(9)	0.539(7)	0.84(1)		
ν (Hz)	0.084748357(2)	0.084738944(1)	0.084728741(1)	0.084721187(1)	0.084717311(2)	0.084712131(3)	0.0847019978(5)		
$\dot{\nu}$ (10^{-13} Hz s $^{-1}$)	-2.85(1)	-2.903(2)	-2.900(1)	-2.921(5)	-2.94(1)	-2.99(1)	-2.936(6)		
$\ddot{\nu}$ (10^{-22} Hz s $^{-2}$)	3(1)	-5.0(7)	6(1)	-	-	5(1)	-		
Residuals (ms)	280.999	183.306	222.007	134.321	92.078	299.326	22.906		

NOTE—S1 to S7 represent the seven time ranges obtained by using the vertical lines in Figure 8 as segmentation points.

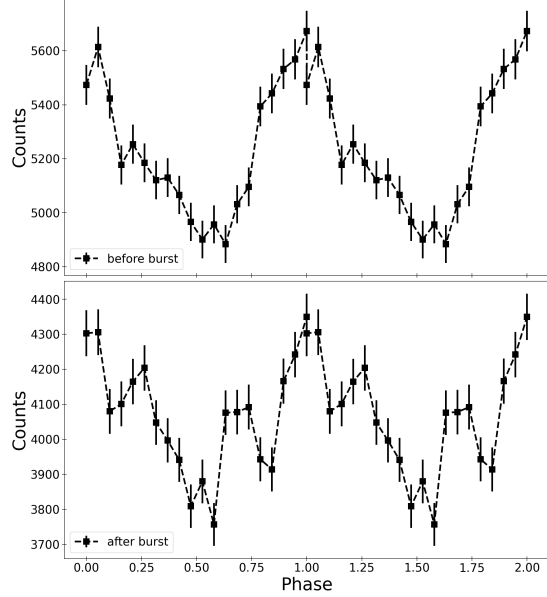


Figure 10. The pulse profile of 1E 1841-045 before (top) and after (bottom) burst, with 20 phase bins. The burst occurred on August 21, 2024, at MJD 60543 (S. Dichiara & D. M. Palmer 2024).

Table 9. The P-value of the chi-square test for pulse profile residuals

Source	S1-S2	S2-S3	S3-S4	S4-S5	S5-S6	S6-S7
1E 2259+586	0.0024	2.2e-8				
4U 0142+61	S1-S2	S2-S3				
χ^2 test	1.2e-6	9.3e-8				
1RXS J1708	S1-S2	S2-S3	S3-S4	S4-S5	S5-S6	S6-S7
χ^2 test	0.090	0.175	0.118	0.155	0.046	0.00010
1E 1841-045	S1-S2	S2-S3	S3-S4	S4-S5	S5-S6	S6-S7
χ^2 test	0.294	0.578	0.073	0.506	0.455	0.020

NOTE—S1-S7 represent the pulse profile in the pulse profile diagram of each source.

Regarding the timing results, there are three thought-provoking points aside from ordinary glitch behaviors. (1) From the current statistics of timing events, the glitch events significantly outnumber the anti-glitch events, which is consistent with previous results. The two new anti-glitch events both occurred in 4U 0142+61, making this source the one with the highest number of such events. Moreover, in this source, anti-glitch events

et al. (2025) analyzed and reported in detail. Therefore, we include this event in Table 10 to provide a complete statistics of timing events within NICER’s monitoring range.

occur more frequently than glitch events, which clearly contradicts the overall statistics of magnetars. What makes this source so unique remains worth further exploration, and exploring the factors behind this difference is crucial for understanding the underlying physical mechanisms. Presumably, the strong crustal toroidal magnetic field contained within the source generates stresses that cause the superfluid vortex lines to move inward, thereby producing anti-glitches. (2) A state transition event occurs in the source 1RXS J1708. This event is similar to the “slow glitch” reported by S. Q. Zhou et al. (2022a), but instead of a spin-up, it involves a spin-down. Whether this gradually evolving event is caused by changes in the magnetic field’s torque and whether it can further constrain theoretical models of magnetars is also worth exploring. Whether this gradually evolving event is caused by changes in the coupling between the external magnetospheric and internal superfluid torques, possibly associated with temperature variations and magnetic-field topology changes that may accompany magnetar bursting activity, and whether it can further constrain theoretical models of magnetars is also worth exploring. (3) The anti-glitch event in 1E 2259+586 is accompanied by an exponential recovery term. This is similar to 4U 0142+61, PSR J1846-0258, and PSR J1119-6127 but differs from SGR J1900+14 and SGR J1935+2154, which show no exponential term (M.-Y. Ge et al. 2024). Regardless, most glitch events are not accompanied by an exponential term. What causes this behavior and how the exponential component may provide for theoretical models are questions that also merit further exploration. One possible explanation for this exponential relaxation after the anti-glitch event is the response of the vortex lines, which creep against the toroidal-arranged flux tubes in the magnetar’s core region, to changes in the crust’s rotation rate.

Also, we study the evolution of the pulse profiles and find that the profiles of 1E 2259+586 and 4U 0142+61 both evolve. This is consistent with the earlier conclusion that evolution appears to be a generic property of magnetars (R. Dib et al. 2008; R. Dib & V. M. Kaspi 2014). However, this type of evolution occurs at a low level and requires the accumulation of sufficiently long pulse profiles to become evident. For 1RXS J1708 and 1E 1841-045, the lack of significant changes in the pulse profiles, compared to those of 1E 2259+586 and 4U 0142+61, may be due to an insufficient signal-to-noise ratio. We calculated the chi-squared values for the significance of the profiles for the latter two, which can be more than ten times smaller than those for the former.

Table 10. Timing Events of Four AXPs Observed by *NICER*

Source	Timing Events	Epoch (MJD)	$\Delta\nu_g$ (Hz)	Profile Change	Reference
1E 2259+586	glitch	57934.48	$1.78(2) \times 10^{-7}$	-	(G. Younes et al. 2020)
1E 2259+586	anti-glitch	58575	$-8.95(5) \times 10^{-8}$	Y ^b	This work ^a , (G. Younes et al. 2020)
1E 2259+586	glitch	59780	$1.935(2) \times 10^{-7}$	Y	This work
4U 0142+61	anti-glitch	59540	$-1.25(9) \times 10^{-8}$	Y	This work
4U 0142+61	anti-glitch	59850	$-5.42(9) \times 10^{-8}$	Y	This work
1RXS J1708	glitch	58755	$1.37(2) \times 10^{-7}$	N	This work
1RXS J1708	glitch	59290	$8.4(2) \times 10^{-8}$	N	This work
1RXS J1708	glitch	59540	$2.9(6) \times 10^{-8}$	N	This work
1RXS J1708	glitch	60200	$2.2(3) \times 10^{-8}$	Y	This work
1RXS J1708	state transition	Around 59800	-	N	This work
1E 1841-045	glitch	60543	$6.1(4) \times 10^{-8}$	Y ^c	(G. Younes et al. 2025)

^a Accompanied by an exponential decay term with $\tau_d = 89(17)$ Days.

^b Possible signs of evolution, but not changes in the pulse profile characteristics.

^c The pulse profile undergoes a significant characteristic change (from a quasi-single-peaked to a complex multi-peaked morphology), accompanied by an outburst.

In 2020, a FRB was discovered to be associated with SGR 1935+2154 (B. Andersen et al. 2020; C. D. Bochenek et al. 2020), leading to the widespread acceptance that magnetars are one of the central engine for the origin for FRBs.. G. Younes et al. (2023) observed that following a spin-down glitch, SGR 1935+2154 emitted three FRB-like radio bursts, followed by pulsed radio radiation lasting for a month. The rarity and near-synchronization of these events suggest a possible connection, providing critical clues about their origin and triggering mechanisms. Additionally, in October 2022, another FRB event occurred from this source, accompanied by two glitch events within nine hours before and after the FRB (C.-P. Hu et al. 2024). The first glitch was associated with a significant increase in burst rate and X-ray flux. However, how magnetars produce FRBs and whether there is a relationship between glitches and FRBs remain unclear. It is worth mentioning that magnetars with radio emissions are very rare, and none of the four magnetars discussed in this paper exhibit radio emission (M. Burgay et al. 2007; W.-J. Lu et al. 2024; J. Bai et al. 2025).

With the improvement of observational capabilities, we have uncovered many phenomenological events related to magnetars. However, these events also raise numerous questions about the physical mechanisms operating in magnetars and even in rotation-powered pulsars. The discovery of anti-glitches in rotation-powered pulsars indicates that such phenomena are not exclusive to magnetars (S. Q. Zhou et al. 2024; Y. L. Tuo et al. 2024). Additionally, two rotation-powered pulsars have now exhibited magnetar-like behaviors, such as activ-

ity accompanied by glitches (S. Dai et al. 2018; R. F. Archibald et al. 2018; R. Sathyaprakash et al. 2024; C.-P. Hu et al. 2023). These observations lead us to consider whether a unified theory of pulsar glitches exists and what role the magnetic field plays in the activity of pulsars. Finally, the current sample of magnetar timing events is still insufficient, and whether there are more peculiar timing behaviors and whether our current statistical understanding holds as the sample size increases remains unknown. Continued systematic monitoring to obtain more samples, especially of rare events, is key to addressing these issues. Excitingly, China is set to launch the enhanced X-ray Timing and Polarimetry mission(eXTP) in the near future (S.-N. Zhang et al. 2025), which will simultaneously provide imaging, timing, and polarimetric analysis of sources (M. Ge et al. 2025). Its unique capabilities are expected to make significant contributions to understanding the physics of magnetars.

ACKNOWLEDGMENTS

The authors thank supports from the National Natural Science Foundation of China under Grants 12473041,12373051. This work is partially supported by the China Manned Space Program with grant no CMS-CSST-2025-A13, the National Key R&D Program of China (2021YFA0718500) from the Minister of Science and Technology of China (MOST) and the China's Space Origins Exploration Program. S.Q.Z. acknowledges support from the Key Project of the Sichuan Science and Technology Education Joint Fund (25LHJJ0097) and the PhD Start-up Fund of China

West Normal University (25KE033). EG is supported by the Doctor Foundation of Qingdao Binhai University (No. BJZA2025025).

REFERENCES

Akbal, O., Gügercioğlu, E., Şaşmaz Muş, S., & Alpar, M. A. 2015, MNRAS, 449, 933, doi: [10.1093/mnras/stv322](https://doi.org/10.1093/mnras/stv322)

An, H., Archibald, R. F., Hascoët, R., et al. 2015, The Astrophysical Journal, 807, 93, doi: [10.1088/0004-637X/807/1/93](https://doi.org/10.1088/0004-637X/807/1/93)

Andersen, B., Bandura, K., & Bhardwaj, M. 2020, Nature, 587, 54, doi: [10.1038/s41586-020-2863-y](https://doi.org/10.1038/s41586-020-2863-y)

Anderson, P. W., & Itoh, N. 1975, Nature, 256, 25, doi: [10.1038/256025a0](https://doi.org/10.1038/256025a0)

Antonopoulou, D., Haskell, B., & Espinoza, C. M. 2022, Reports on Progress in Physics, 85, 126901, doi: [10.1088/1361-6633/ac9ced](https://doi.org/10.1088/1361-6633/ac9ced)

Archibald, R. F., Kaspi, V. M., Scholz, P., et al. 2017, The Astrophysical Journal, 834, 163, doi: [10.3847/1538-4357/834/2/163](https://doi.org/10.3847/1538-4357/834/2/163)

Archibald, R. F., Kaspi, V. M., Tendulkar, S. P., & Scholz, P. 2018, The Astrophysical Journal, 869, 180, doi: [10.3847/1538-4357/aaee73](https://doi.org/10.3847/1538-4357/aaee73)

Archibald, R. F., Kaspi, V. M., Ng, C. Y., et al. 2013, Nature, 497, 591, doi: [10.1038/nature12159](https://doi.org/10.1038/nature12159)

Bai, J., Wang, N., Dai, S., et al. 2025, The Astrophysical Journal, 979, 122, doi: [10.3847/1538-4357/ada3c4](https://doi.org/10.3847/1538-4357/ada3c4)

Baldini, L., Bucciantini, N., Lalla, N. D., et al. 2022, SoftwareX, 19, 101194, doi: <https://doi.org/10.1016/j.softx.2022.101194>

Bochenek, C. D., Ravi, V., & Belov, K. V. 2020, Nature, 587, 59, doi: [10.1038/s41586-020-2872-x](https://doi.org/10.1038/s41586-020-2872-x)

Burgay, M., Rea, N., & Israel, G. e. a. 2007, Astrophysics and Space Science, 308, 521. <https://doi.org/10.1007/s10509-007-9353-7>

Coti Zelati, F., Rea, N., Pons, J. A., Campana, S., & Esposito, P. 2017, Monthly Notices of the Royal Astronomical Society, 474, 961, doi: [10.1093/mnras/stx2679](https://doi.org/10.1093/mnras/stx2679)

Dai, S., Johnston, S., Weltevrede, P., et al. 2018, Monthly Notices of the Royal Astronomical Society, 480, 3584, doi: [10.1093/mnras/sty2063](https://doi.org/10.1093/mnras/sty2063)

Dib, R., & Kaspi, V. M. 2014, ApJ, 784, 37, doi: [10.1088/0004-637X/784/1/37](https://doi.org/10.1088/0004-637X/784/1/37)

Dib, R., Kaspi, V. M., & Gavriil, F. P. 2008, The Astrophysical Journal, 673, 1044, doi: [10.1086/524653](https://doi.org/10.1086/524653)

Dichiara, S., & Palmer, D. M. 2024, The Astronomer's Telegram, 16784, 1

Esposito, P., Rea, N., & Israel, G. L. 2021, Magnetars: A Short Review and Some Sparse Considerations, ed. T. M. Belloni, M. Méndez, & C. Zhang (Berlin, Heidelberg: Springer Berlin Heidelberg), 97–142, doi: [10.1007/978-3-662-62110-3_3](https://doi.org/10.1007/978-3-662-62110-3_3)

Fahlman, G. G., & Gregory, P. C. 1981, Nature, 293, 202, doi: [10.1038/293202a0](https://doi.org/10.1038/293202a0)

Ferdman, R. D., Archibald, R. F., & Kaspi, V. M. 2015, The Astrophysical Journal, 812, 95, doi: [10.1088/0004-637X/812/2/95](https://doi.org/10.1088/0004-637X/812/2/95)

Gavriil, F. P., Dib, R., & Kaspi, V. M. 2011a, The Astrophysical Journal, 736, 138, doi: [10.1088/0004-637X/736/2/138](https://doi.org/10.1088/0004-637X/736/2/138)

Gavriil, F. P., Kaspi, V. M., & Woods, P. M. 2002, Nature, 419, 142, doi: [10.1038/nature01011](https://doi.org/10.1038/nature01011)

Ge, M., Yang, Y.-P., Lu, F., et al. 2022, <https://arxiv.org/abs/2211.03246>

Ge, M., Ji, L., Taverna, R., et al. 2025, arXiv e-prints, arXiv:2506.08369, doi: [10.48550/arXiv.2506.08369](https://doi.org/10.48550/arXiv.2506.08369)

Ge, M. Y., Lu, F. J., Qu, J. L., et al. 2012, The Astrophysical Journal Supplement Series, 199, 32, doi: [10.1088/0067-0049/199/2/32](https://doi.org/10.1088/0067-0049/199/2/32)

Ge, M.-Y., Yang, Y.-P., Lu, F.-J., et al. 2024, Research in Astronomy and Astrophysics, 24, 015016, doi: [10.1088/1674-4527/ad0f0c](https://doi.org/10.1088/1674-4527/ad0f0c)

Gendreau, K. C., Arzoumanian, Z., & Adkins, P. W. 2016, in Space Telescopes and Instrumentation 2016: Ultraviolet to Gamma Ray, ed. J.-W. A. den Herder, T. Takahashi, & M. Bautz, Vol. 9905, International Society for Optics and Photonics (SPIE), 99051H, doi: [10.1117/12.2231304](https://doi.org/10.1117/12.2231304)

Giacconi, R., Murray, S., Gursky, H., et al. 1972, ApJ, 182, 281, doi: [10.1086/151790](https://doi.org/10.1086/151790)

Gügercioğlu, E. 2017, MNRAS, 469, 2313, doi: [10.1093/mnras/stx985](https://doi.org/10.1093/mnras/stx985)

Gügercioğlu, E., & Alpar, M. A. 2016, MNRAS, 462, 1453, doi: [10.1093/mnras/stw1758](https://doi.org/10.1093/mnras/stw1758)

Gügercioğlu, E., Köksal, E., & Güver, T. 2023, MNRAS, 518, 5734, doi: [10.1093/mnras/stac3516](https://doi.org/10.1093/mnras/stac3516)

Gügercioğlu, E., & Alpar, M. A. 2017, MNRAS, 471, 4827, doi: [10.1093/mnras/stx1937](https://doi.org/10.1093/mnras/stx1937)

Gügercioğlu, E., & Alpar, M. A. 2019, MNRAS, 488, 2275, doi: [10.1093/mnras/stz1831](https://doi.org/10.1093/mnras/stz1831)

Hobbs, G. B., Edwards, R. T., & Manchester, R. N. 2006, *MNRAS*, 369, 655, doi: [10.1111/j.1365-2966.2006.10302.x](https://doi.org/10.1111/j.1365-2966.2006.10302.x)

Hu, C.-P., Narita, T., Enoto, T., & Younes, G. 2024, *Nature*, 626, 500, doi: [10.1038/s41586-023-07012-5](https://doi.org/10.1038/s41586-023-07012-5)

Hu, C.-P., Kuiper, L., Harding, A. K., et al. 2023, *The Astrophysical Journal*, 952, 120, doi: [10.3847/1538-4357/acd850](https://doi.org/10.3847/1538-4357/acd850)

Israel, Götz, D., Zane, S., et al. 2007, *A&A*, 476, L9, doi: [10.1051/0004-6361:20078215](https://doi.org/10.1051/0004-6361:20078215)

Israel, G. L., Mereghetti, S., & Stella, L. 1994, *ApJL*, 433, L25, doi: [10.1086/187539](https://doi.org/10.1086/187539)

Kaspi, V. M., & Beloborodov, A. M. 2017, *ARA&A*, 55, 261, doi: [10.1146/annurev-astro-081915-023329](https://doi.org/10.1146/annurev-astro-081915-023329)

Kaspi, V. M., & Gavriil, F. P. 2003b, *The Astrophysical Journal*, 596, L71, doi: [10.1086/379093](https://doi.org/10.1086/379093)

Kaspi, V. M., Gavriil, F. P., Woods, P. M., et al. 2003, *The Astrophysical Journal*, 588, L93, doi: [10.1086/375683](https://doi.org/10.1086/375683)

Kaspi, V. M., Lackey, J. R., & Chakrabarty, D. 2000, *The Astrophysical Journal*, 537, L31, doi: [10.1086/312758](https://doi.org/10.1086/312758)

Livingstone, M. A., Kaspi, V. M., & Gavriil, F. P. 2005, *The Astrophysical Journal*, 633, 1095, doi: [10.1086/491643](https://doi.org/10.1086/491643)

Lower, M. E., Johnston, S., Dunn, L., et al. 2021, *Monthly Notices of the Royal Astronomical Society*, 508, 3251, doi: [10.1093/mnras/stab2678](https://doi.org/10.1093/mnras/stab2678)

Lu, W.-J., Zhou, P., Wang, P., et al. 2024, *The Astrophysical Journal*, 963, 151, doi: [10.3847/1538-4357/ad27cf](https://doi.org/10.3847/1538-4357/ad27cf)

Lyutikov, M. 2013, arXiv, doi: [10.48550/arXiv.1306.2264](https://doi.org/10.48550/arXiv.1306.2264)

Mazets, E. P., & Golenetskii, S. V. 1979b, *Nature*, 282, 287, doi: [10.1038/282587a0](https://doi.org/10.1038/282587a0)

Mazets, E. P., Golenetskij, S. V., & Guryan, Y. A. 1979a, *Soviet Astronomy Letters*, 5, 343

Olausen, S. A., & Kaspi, V. M. 2014, *ApJS*, 212, 6, doi: [10.1088/0067-0049/212/1/6](https://doi.org/10.1088/0067-0049/212/1/6)

Peng, H. L., Ge, M. Y., & Weng, S. S. 2024, *The Astrophysical Journal*, 961, 106, doi: [10.3847/1538-4357/ad1512](https://doi.org/10.3847/1538-4357/ad1512)

Pines, D., & Alpar, M. A. 1985, *Nature*, 316, 27, doi: [10.1038/316027a0](https://doi.org/10.1038/316027a0)

Ray, P. S., Guillot, S., Ho, W. C. G., et al. 2019, *The Astrophysical Journal*, 879, 130, doi: [10.3847/1538-4357/ab24d8](https://doi.org/10.3847/1538-4357/ab24d8)

Rea, N., & Esposito, P. 2011, in *High-Energy Emission from Pulsars and their Systems*, ed. D. F. Torres & N. Rea (Berlin, Heidelberg: Springer Berlin Heidelberg), 247–273

Rigoselli, M., Taverna, R., Mereghetti, S., et al. 2025, *The Astrophysical Journal Letters*, 985, L34, doi: [10.3847/2041-8213/adbff](https://doi.org/10.3847/2041-8213/adbff)

Sathyaprakash, R., Rea, N., Coti Zelati, F., et al. 2024, *The Astrophysical Journal*, 976, 56, doi: [10.3847/1538-4357/ad8226](https://doi.org/10.3847/1538-4357/ad8226)

Scholz, P., Archibald, R. F., Kaspi, V. M., et al. 2014, *The Astrophysical Journal*, 783, 99, doi: [10.1088/0004-637X/783/2/99](https://doi.org/10.1088/0004-637X/783/2/99)

Stewart, R., Younes, G. A., Harding, A. K., et al. 2025, *The Astrophysical Journal Letters*, 985, L35, doi: [10.3847/2041-8213/adbff](https://doi.org/10.3847/2041-8213/adbff)

Sugizaki, M., Nagase, F., Torii, K., et al. 1997, *Publications of the Astronomical Society of Japan*, 49, L25, doi: [10.1093/pasj/49.5.L25](https://doi.org/10.1093/pasj/49.5.L25)

Thompson, C., & Duncan, R. C. 1995, *Monthly Notices of the Royal Astronomical Society*, 275, 255, doi: [10.1093/mnras/275.2.255](https://doi.org/10.1093/mnras/275.2.255)

Thompson, C., & Duncan, R. C. 1996, *The Astrophysical Journal*, 473, 322, doi: [10.1086/178147](https://doi.org/10.1086/178147)

Thompson, C., Duncan, R. C., Woods, P. M., et al. 2000, *ApJ*, 543, 340, doi: [10.1086/317072](https://doi.org/10.1086/317072)

Tong, H. 2014, *The Astrophysical Journal*, 784, 86, doi: [10.1088/0004-637X/784/2/86](https://doi.org/10.1088/0004-637X/784/2/86)

Tong, H. 2023, Magnetospheric physics of magnetars, <https://arxiv.org/abs/2309.05181>

Tuo, Y. L., Serim, M. M., Antonelli, M., et al. 2024, *The Astrophysical Journal Letters*, 967, L13, doi: [10.3847/2041-8213/ad4488](https://doi.org/10.3847/2041-8213/ad4488)

Turolla, R., Zane, S., & Watts, A. L. 2015, *Reports on Progress in Physics*, 78, 116901, doi: [10.1088/0034-4885/78/11/116901](https://doi.org/10.1088/0034-4885/78/11/116901)

Vasisht, G., & Gotthelf, E. V. 1997, *The Astrophysical Journal*, 486, L129, doi: [10.1086/310843](https://doi.org/10.1086/310843)

Wong, T., Backer, D. C., & Lyne, A. G. 2001, *The Astrophysical Journal*, 548, 447, doi: [10.1086/318657](https://doi.org/10.1086/318657)

Woods, P. M., Kaspi, V. M., Thompson, C., et al. 2004, *The Astrophysical Journal*, 605, 378, doi: [10.1086/382233](https://doi.org/10.1086/382233)

Younes, G., Baring, M. G., Harding, A. K., & Enoto, T. 2023, *Nature Astronomy*, 7, 339, doi: [10.1038/s41550-022-01865-y](https://doi.org/10.1038/s41550-022-01865-y)

Younes, G., Lander, S. K., & Baring, M. G. 2025, arXiv, doi: [10.48550/arXiv.2502.20079](https://doi.org/10.48550/arXiv.2502.20079)

Younes, G., Ray, P. S., Baring, M. G., et al. 2020, *The Astrophysical Journal Letters*, 896, L42, doi: [10.3847/2041-8213/ab9a48](https://doi.org/10.3847/2041-8213/ab9a48)

Zhang, S.-N., Santangelo, A., Xu, Y., et al. 2025, arXiv e-prints, arXiv:2506.08101, doi: [10.48550/arXiv.2506.08101](https://doi.org/10.48550/arXiv.2506.08101)

Zhou, S. Q., Gügercioğlu, E., Yuan, J., Ge, M., & Yu, C. 2022a, *Universe*, 8, doi: [10.3390/universe8120641](https://doi.org/10.3390/universe8120641)

Zhou, S. Q., Ye, W. T., Ge, M. Y., et al. 2024, The Astrophysical Journal, 977, 243,
doi: [10.3847/1538-4357/ad938d](https://doi.org/10.3847/1538-4357/ad938d)

Zhou, S. Q., Gügencinoğlu, E., Yuan, J. P., et al. 2022b, Monthly Notices of the Royal Astronomical Society, 519, 74, doi: [10.1093/mnras/stac3355](https://doi.org/10.1093/mnras/stac3355)

İçdem, B., Baykal, A., & İnam, S. Ç. 2012, Monthly Notices of the Royal Astronomical Society, 419, 3109,
doi: [10.1111/j.1365-2966.2011.19953.x](https://doi.org/10.1111/j.1365-2966.2011.19953.x)

Şaşmaz Muş, S., Aydin, B., & Göğüş, E. 2014, Monthly Notices of the Royal Astronomical Society, 440, 2916,
doi: [10.1093/mnras/stu436](https://doi.org/10.1093/mnras/stu436)